Journal of Molecular Graphics and Modelling 38 (2012) 123–136

Contents lists available at SciVerse ScienceDirect

Journal of Molecular Graphics and Modelling

journal homepage: www.elsevier.com/locate/JMGM

Impact of the CXCR4 structure on docking-based virtual screening of HIV entry inhibitors

Jesús M. Planesas[a,1], Violeta I. Pérez-Nueno[a,b,*], José I. Borrell[a,1], Jordi Teixidó[a,1]

[a] Grup d'Enginyeria Molecular, Institut Químic de Sarriá (IQS), Universitat Ramon Llull, Barcelona, Spain
[b] INRIA Nancy, LORIA, 615 rue du Jardin Botanique, 54600 Villers-lès-Nancy, France

ARTICLE INFO

Article history:
Accepted 25 June 2012
Available online 3 July 2012

Keywords:
CXCR4
Retrospective docking-based screening
Early recovery
Scaffold retrieval

ABSTRACT

Herein we analyze in depth the receptor-based virtual screening (VS) performance of the five recent crystallized CXCR4 structures along with a CXCR4 rhodopsin-based homology model. All CXCR4 Protein Data Bank (PDB) structures are co-crystallized with a small organic antagonist except structure 3OE0, which is co-crystallized with a cyclic peptide analog. Evaluation of the CXCR4 models was done by retrospective docking-based VS using a test set of 248 known CXCR4 inhibitors from 4 different chemotype families and 4696 different presumed inactives. The performance of the docking protocol using the five different protein structures was assessed in terms of pose prediction and hits detection using 12 different docking scoring functions and a scoring function with rescoring. Results show that 3OE6 structure achieves the highest docking-based performance with an average area under the curve (aAUC) of 0.84 and an average enrichment factor (aEF) of 11.7 at 1% of decoys screened. CXCR4 rhodopsin-like homology model performs comparable to the crystallized structures in the 1% of database screened. Moreover, a detailed analysis of the retrospective docking results using the CXCR4 homology model in Discovery Studio allows us to hypothesize the existence of multiple binding sub-sites in CXCR4 binding pocket.

1. Introduction

HIV cell infection is a multi-stage and complex process. It starts with the virus entry [1] into the host membrane. The first stage of the entry process is the virus attachment to the cell membrane through receptor CD4. Secondly, viral proteins *gp120* [2] and *gp41* bind to the co-receptors CCR5 and CXCR4 [3] to facilitate virus anchoring to the host cellular membrane. Finally, the viral envelope undergoes conformational changes that allow the insertion of the *gp41* fusion peptide into the host membrane.

One of the strategies to block the HIV entry process is inhibiting the binding of the viral protein *gp120* to the co-receptors CXCR4 or CCR5. The first interaction between *gp120* and these co-receptors is through their extracellular loops. CXCR4 and CCR5 are both chemokine receptors which belong to the GPCR superfamily [4] and are implicated in a wide range of human diseases [5]. This subfamily of GPCR proteins is responsible for transmitting signals from the extracellular environment as well as the recognition of extracellular ligands. All GPCRs have a common characteristic structure relatively hydrophobic with 7 transmembrane domains. The N-terminus is located in the extracellular side and the transmembrane helices are connected by three extracellular loops whereas the C-terminus is located in the intracellular side facing the cytoplasm and three intracellular loops connect the interior domain of the transmembrane helices (Fig. 1). The transmembrane helices are expanded in the plasmatic membrane as anticlockwise bundle of alpha-helices. Therefore extracellular loops fulfill important roles in receptor activation and consequently in ligand binding [6].

An important achievement was accomplished at the end of 2010 when Wu et al. [7] crystallized five independent CXCR4 structures with a resolution of 2.5–3.2 Å (Table 1). These crystal structures contain a small organic molecule derived from isothiourea [8] (IT1t) in Protein Data Bank structures (PDBs) 3ODU, 3OE6, 3OE8 and 3OE9, and a 16-residue cyclic peptide [9] (CVX15) in PDB 3OE0, as antagonists bound to the CXCR4 structure.

In all the PDBs we can observe that the ligand binding site is located in the second extracellular loop, ECL2, close to the N-terminus (Fig. 2). Also, superposition of ligand binding pockets shows similar overlapping volume. The residues that induce common interactions in both ligands are Tyr116, Asp187 and Glu288 (Fig. 3). Those residues are common in CXCR4 antagonist binding as it has been widely discussed in previous literature

* Corresponding author at: INRIA Nancy, LORIA, 615 rue du Jardin Botanique, 54600 Villers-lès-Nancy, France. Tel.: +33 3 83593045/+34 93 267 20 00; fax: +33 3 83413079/+34 93 205 62 66.
E-mail addresses: violeta.pereznueno@inria.fr, violeta.perez@iqs.url.edu (V.I. Pérez-Nueno), jordi.teixido@iqs.edu (J. Teixidó).
[1] Tel.: +34 93 267 20 00; fax: +34 93 205 62 66.

1093-3263/$ – see front matter © 2012 Elsevier Inc. All rights reserved.
http://dx.doi.org/10.1016/j.jmgm.2012.06.010

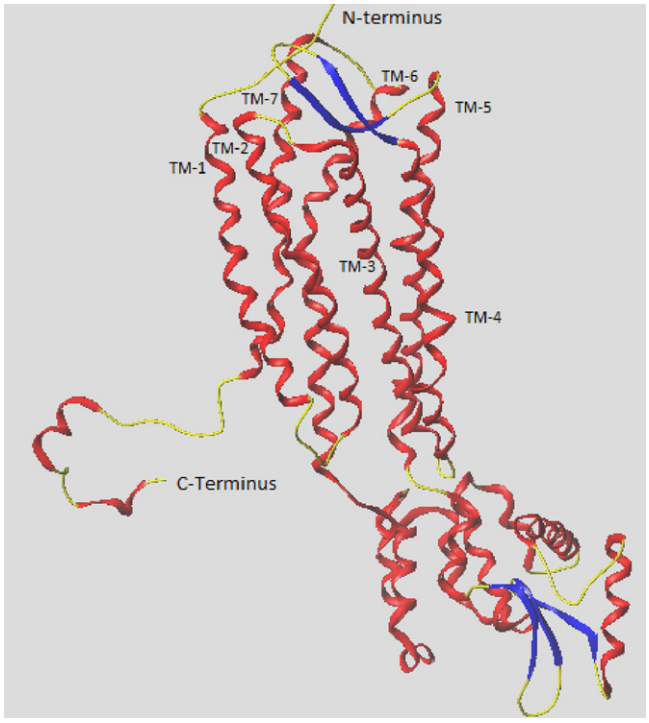

Fig. 1. Backbone scheme of the co-receptor CXCR4 composed by the seven typical GPCR transmembrane domains, the intracellular C-terminus and the extracellular N-terminus with their corresponding triad of extracellular and intracellular loops.

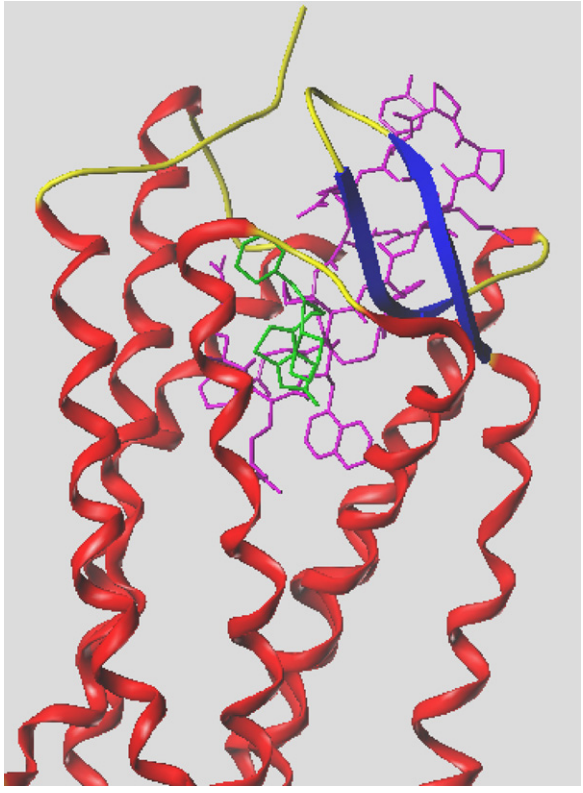

Fig. 2. CXCR4 ligand binding pocket complexed with the small organic antagonist IT1t, colored in green, superimposed with the structure of the peptide ligand CVX15, colored in purple. (For interpretation of the references to color in this figure legend, the reader is referred to the web version of the article.)

Table 1
Resolution and characteristics of CXCR4 structures published by Wu et al.

PDB	Resolution (Å)	Ligand	Receptor units
3ODU	2.5	IT1t	Dimeric CXCR4
3OE0	2.9	CVX15	Monomeric CXCR4
3OE6	3.2	IT1t	Monomeric CXCR4
3OE8	3.1	IT1t	Trimeric CXCR4
3OE9	3.1	IT1t	Dimeric CXCR4

[10,11]. Although the overall orientation differs between ligands, hydrophobic interactions highly contribute in the binding affinity of the majority of CXCR4 antagonists. The residues Ala95, Leu91, Val112, His113, Tyr116, Phe292, Tyr255 and Ile259 play important roles in hydrophobic binding. Moreover, Tyr45 on TM1, Trp94 and Asp97 on TM2, Tyr116 on TM3, Asp171 on TM4, Asp262 on TM6 and His281 and Glu288 on TM7, are critical residues involved in stabilizing interactions with known CXCR4 antagonists [12–14]

Nevertheless, in the case of the peptide ligand it is observed a ligand-induced conformational change in the extracellular side of the helix 5 [7]. Hence, the docking-based virtual screening (VS) of small peptides might be more dependent on the CXCR4 structure used for the screening.

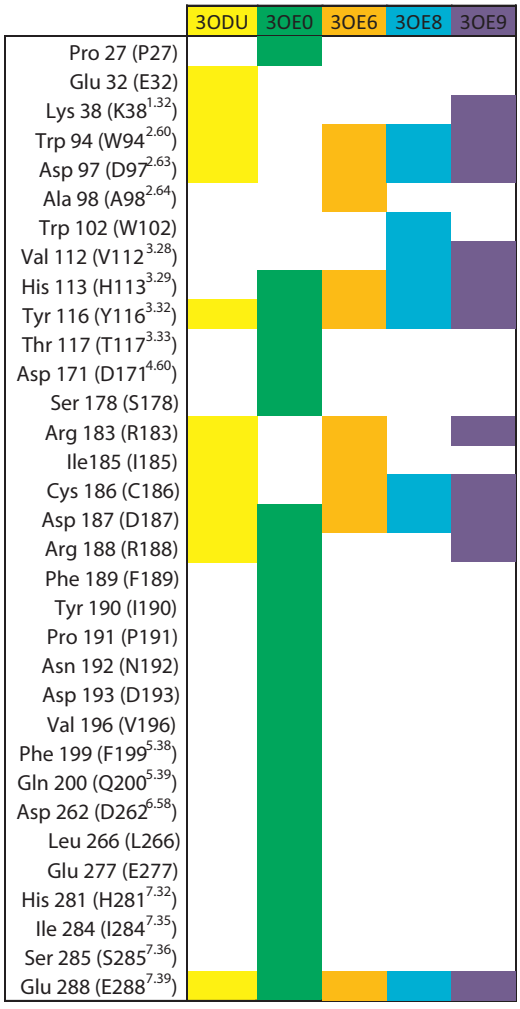

Fig. 3. Protein–ligand interaction map for each complex structure. Structure 3OE0, whose co-crystallized ligand CVX15 has a large volume presents, many protein–ligand interactions in comparison with the rest of complexes whose common co-crystallized ligand IT1t is smaller. Some different interactions can be appreciated between PDBs 3ODU, 3OE6, 3OE8, 3OE9. However, superposition of crystallized IT1t binding modes is very similar in all cases. In brackets Ballesteros–Weinstein residues notation [65].

2. Methods

2.1. Virtual screening data preparation

In the last years GPCR and also chemokine receptors have begun to be determined successfully by protein crystallography. In the case of the chemokine co-receptor CXCR4, Wu et al. obtained five CXCR4 structures at the end of 2010.

We analyzed the five CXCR4 structures published in the Protein Data Bank by retrospective docking-based (VS) using different representative force-filed based, empirical, and knowledge-based scoring functions [15]: AutoDock Vina [16] from AutoDock, GoldScore [17], ChemScore [17] and GoldScore rescored with ChemScore from Gold 4.1, Glide 5.5 [18], TotalScore provided in Surflex [19] from Sybyl X 1.1 [20], Ligandfit scoring functions (LigScore1; LigScore2 [21]; PLP1; PLP2 [22,23]; Jain [23], PMF and Dock_Score) implemented in Discovery Studio 2.5.

Moreover, we compared these results with the ones retrieved by our previously published CXCR4 rhodopsin-based homology model built when there were not available CXCR4 crystal structures [24]. This homology model agrees with the folding structure of the crystal PDBs now available. Fig. 4 shows the superposition of our homology model and the crystal CXCR4 structure 3ODU. A detailed structural comparison between homology models and CXCR4 crystal structures was done by Kufareva et al. [25]. Herein, we compare our homology model against the crystal structures in terms of retrospective docking performance, especially the early recovery.

To perform the retrospective docking-based screening we used the test set of Pérez-Nueno et al. [24]. This test set contains 248 inhibitors representative of 4 CXCR4 antagonist scaffold families [8,26] (Fig. 5) and 4696 different presumed inactives extracted [24] from the Maybridge Screening Collection whose physicochemical properties (molecular weight, number of rotatable single bonds,

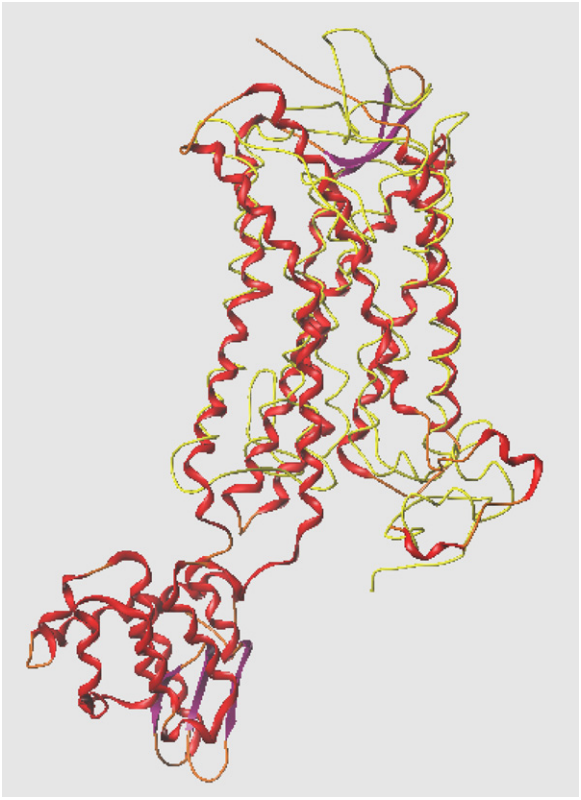

Fig. 4. Superposition of CXCR4 structures PDB 3ODU (red) and the homology model (yellow). Residues Asp171, Asp262 and Glu288 have been used to define superposition. (For interpretation of the references to color in this figure legend, the reader is referred to the web version of the article.)

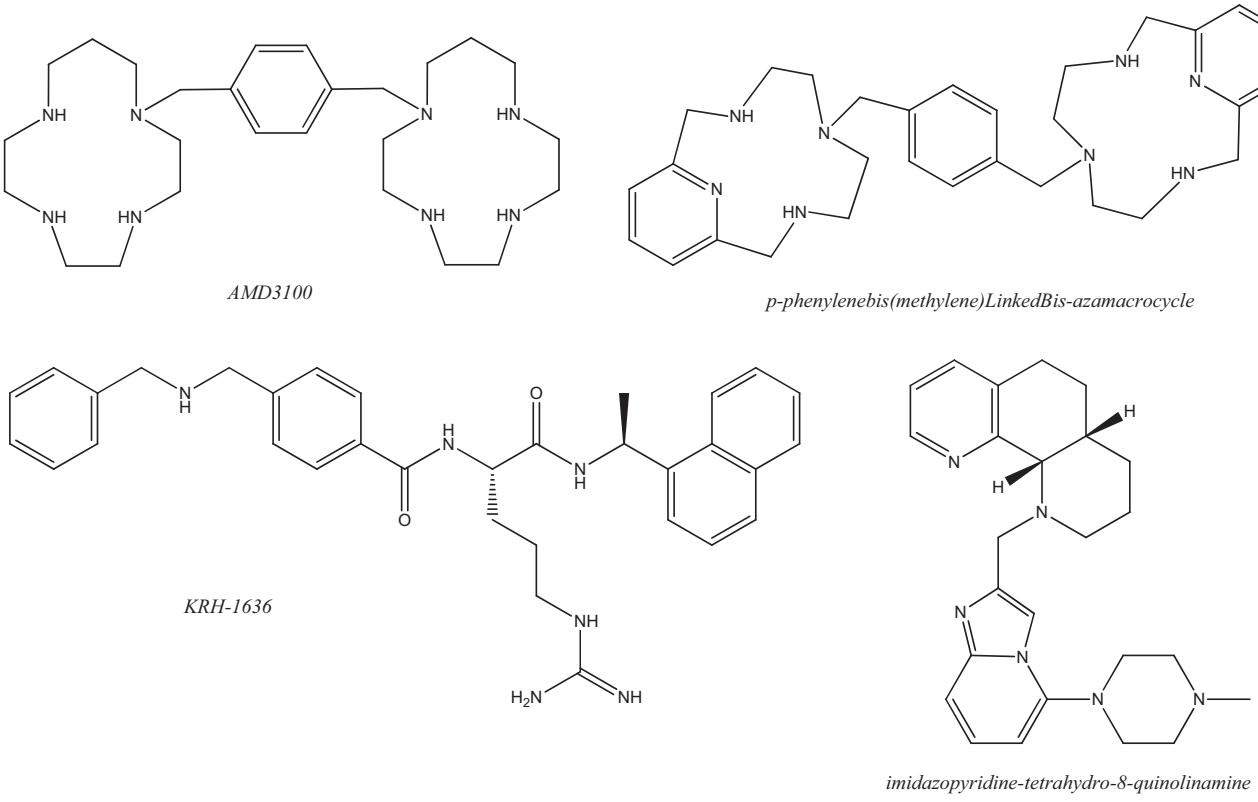

Fig. 5. Representative compounds of the chemotype families used as actives in the test set 24 to guarantee diversity of true binders.

Table 2
Ligands and decoys molecular properties: summary of the 1D physicochemical properties of active and decoy molecules. Standard deviation values in parentheses.

	Ligands: 248	Decoys: 4549
Molecular weight	727.1/306.5 (74.3)	613.9/452.2 (34.9)
Rotatable single bonds	18/0 (4.0)	24/0 (2.2)
Number of hydrogen-bond acceptor atoms	6/1 (1.2)	13/0 (1.6)
Number of hydrogen-bond donor atoms	5/0 (1.3)	9/0 (1.0)
Number of hydrophobic atoms	46/15 (4.6)	43/9 (3.7)
Octanol–water partition coefficient	7.6/−2.8 (2.3)	13.9/−2.8 (1.8)
Polar surface area	485.5/25.8 (60.0)	561.5/0.0 (91.7)
Total positive partial charges	18.58/5.99 (1.24)	12.14/0.69 (2.34)
Total negative partial charges	−4.33/−13.8 (1.16)	−0.69/−10.79 (1.35)

number of hydrogen-bond acceptor atoms, number of hydrogen-bond donor atoms, octanol–water partition coefficient, number of hydrophobic atoms, PSA, total positive partial charges and total negative partial charges) match similar property values than the selected actives [27]. Table 2 shows that the average and standard deviations of these properties calculated by MOE 2009 [28] are quite similar for the active and inactive pools. Supplementary Fig. 1 shows the ROC curves obtained when ligands and decoys were classified by their total positive partial charge (PEOE PC+), total negative partial charge (PEOE PC−), total polar surface area (TPSA) and log octanol/water partition coefficient (log *P*) in order to evaluate the relevance of the decoy set. It can be seen that TPSA, log *P* and PEOE PC− discriminate randomly actives from decoys, as expected in a proper selection of a decoy set. However, the PEOE PC+ ROC curve favors actives retrieval given that the total positive partial charge distribution for the decoy set is a bit lower than the active ligand set.

Both ligands and decoys were protonated at physiological pH, Gasteiger partial charges were assigned and geometric structure was minimized using MMFF94 forcefield implemented in MOE.

Protein structures were prepared prior to their docking, using the own protein preparation module implemented in each docking tool: for AutoDock Vina we used *ADT program* to prepare the corresponding PDBQT-protein file, *Protein Setup* tool was used for Gold, *Protein Preparation Wizard* for Glide, *Prepare Protein Structure* for Sybyl and *Prepare Protein* in the case of Discovery Studio. The protein structure was protonated and minimized using forcefields: OPLS2005, TRIPOS and CHARMm for Glide, Sybyl X and Discovery Studio protocols respectively. His281 and His113, allocated in the near boundaries outside the binding site definition, were protonated equally in all preparation programs. Redundant homodimeric and homotrimeric chains were suppressed. Only the larger chains with less gaps in the binding pocket region were kept in order to avoid gaps inserted between residues known to make important interactions with the bound ligand (for example, in 3ODU structure, the second shortest protein chain lacks the Pro27, which presents a direct interaction with the peptidic ligand in structure 3OE0 (Fig. 3)); a second example is the central monomeric unit in structure 3OE8 which presents gaps corresponding to residues Leu267, Glu268, Ile269, Ile270 and Lys271. These residues do not interact with the small ligand IT1t, but in the case of ligand CVX15 they are allocated much closer to the peptidic ligand and taking into account that CXCR4 has a deep binding pocket it seems convenient not to underestimate. A third example is one of the chains in structure 3OE9 which starts from the residue 35 and presents gaps corresponding to residues Cys28, Phe29, Arg30, Asn31, and gaps as well corresponding to residues Gln66, Lys67, Lys68 and Leu69. Again in this case, residues Cys28, Phe29, Arg30 and Asn31 are placed very close to the ligand CVX15 and in a deep and big binding site these residues could interact with other CXCR4 ligands. Additionally, water molecules present only in PDBs 3ODU and 3OE0, as well as chemical molecules used as crystallization aiders, were eliminated. For structure 3ODU, binding site water molecules were both kept and eliminated for comparison purposes.

CXCR4 binding pocket was defined setting the volume, where the ligands could interact with the protein, delimited by residues Asp171, Asp262 and Glu288 (Fig. 6). Several mutagenic studies confirm interactions between Asp171, Asp262 and Glu288 residues with different ligands such as bicyclam AMD3100 [29–31], monocyclams AMD3465 and AMD3529 [32] or non cyclams like AMD070 [10] in different ways. This triad of acidic residues also interacts with peptidic ligands like T-140 a 14-residue polypeptide [33,34] or cyclopentapeptides antagonists like FC131 and their derivates [35].

2.2. Retrospective docking-based virtual screening

We docked Pérez-Nueno et al. test set of actives and decoys onto each CXCR4 PDB and the CXCR4 homology model using the aforementioned 12 scoring functions and the scoring function with rescoring. All the screened compounds were ranked by their retrieved scores and the final ranking lists were represented in a ROC plot [36]. The area under the ROC plot (AUC) [36,37] and the normalized partial area under the curve, or partial area index, were quantified to evaluate the VS performance. As high AUC values do not guarantee that the top ranked poses will correspond to active compounds [38], we calculated the partial area under the curve [39,40] (pAUC) at 1%, 5% and 10% of false positives. The corresponding values were normalized to partial area indexes [41].

$$\mathrm{pAUC}_{x\%} = \frac{1}{2}\left[1 + \frac{\mathrm{AUC}_{x\%} - \mathrm{AUC}_{\text{random at } x\%}}{\mathrm{AUC}_{\text{perfect at } x\%} - \mathrm{AUC}_{\text{random at } x\%}}\right]$$

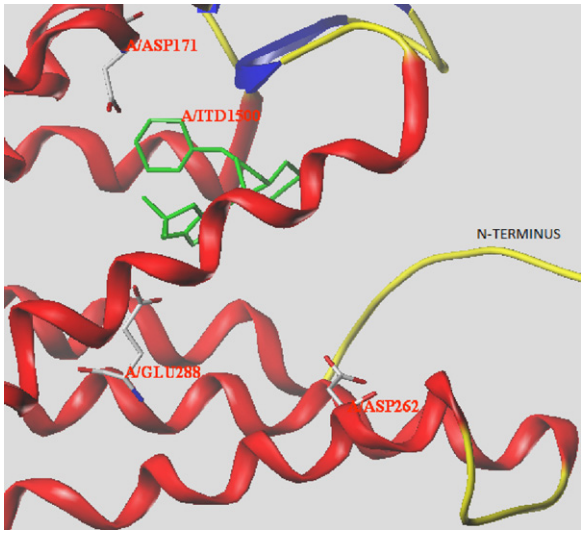

Fig. 6. Definition of the CXCR4 binding site by residues Asp171, Asp262 and Glu288 in the N-terminus region. The small co-crystallized ligand IT1t is shown in green color. It is allocated on one side of the pocket making interactions with Asp171 residue. (For interpretation of the references to color in this figure legend, the reader is referred to the web version of the article.)

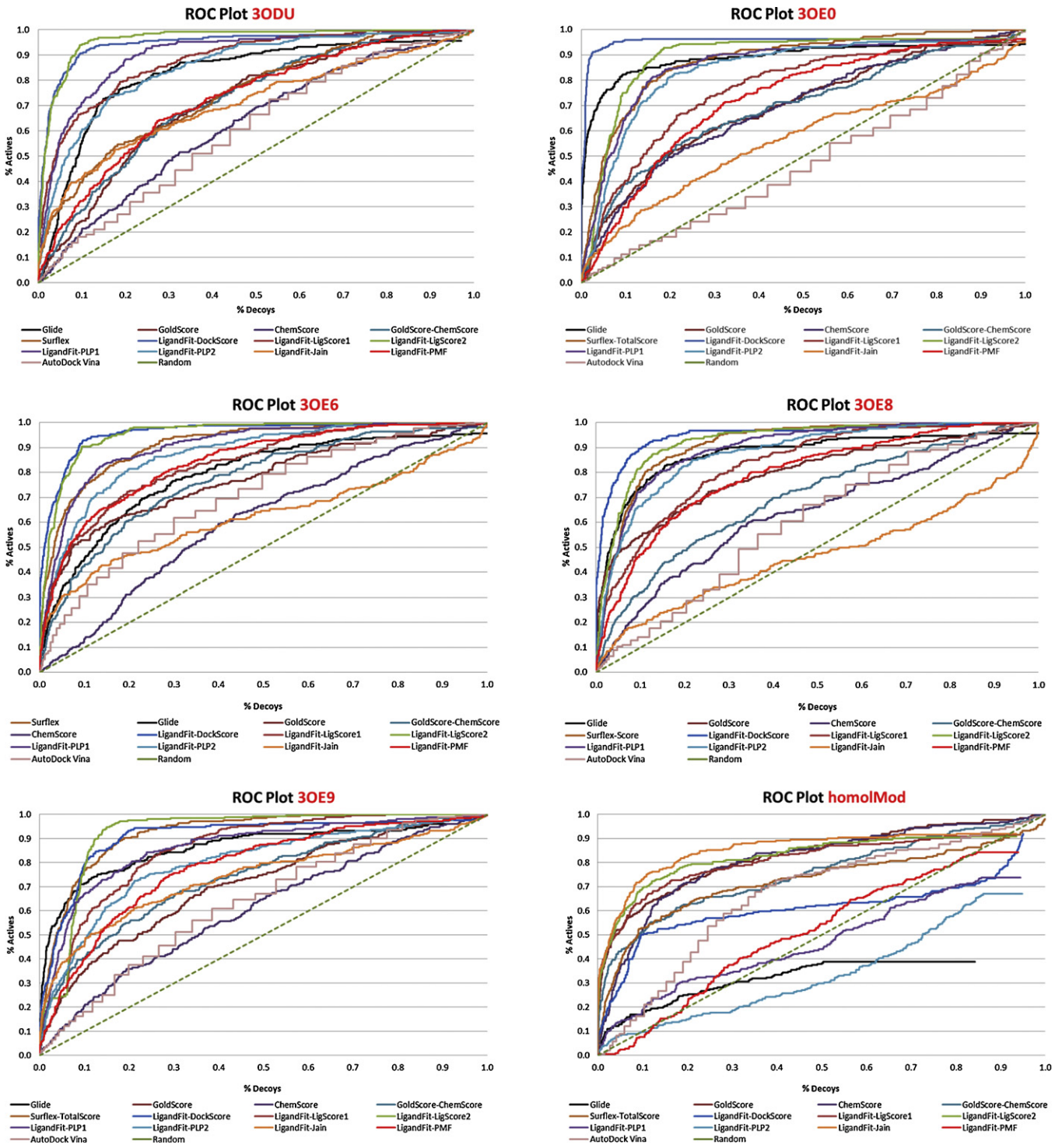

Fig. 7. ROC plots of the retrospective docking-based VS of Pérez-Nueno et al. CXCR4 test set for each of the five experimental CXCR4 structures and the CXCR4 homology model.

In order to compare the overall AUC and the pAUC values obtained for each structure we calculate the average area under the curve (aAUC) as well as the average pAUC of all scoring functions for each PDB.

Furthermore, evaluation [42] of early recovery of actives was assessed by the enrichment factor (EF) [43] at 1%, 5% and 10% of screened database and, additionally, by the percentage of actives retrieved at 1%, 5% and 10% of decoys. Moreover, the average enrichment factor (aEF) at 1%, 5% and 10% of database screened, and the average of the percentage of true positives retrieved at 1%, 5% and 10% of decoys were also calculated based in all 13 scoring functions used in the analysis.

2.3. Accuracy in pose prediction and docking reliability

The accuracy in pose prediction was evaluated by selfdocking the CXCR4 PDBs containing the same cognate ligand using the aforementioned scoring functions under the same docking

conditions [44]. This allows the analysis of possible geometric and shape differences between CXCR4 structures.

The docking reliability was evaluated for each CXCR4 complex by calculating the root-mean square-deviation (RMSD) between the position of the co-crystallized ligand, taken as the reference, and the binding mode predicted by the docking function, also by the best docked pose (taken as the one with the lowest RMSD with respect to the crystal structure), the average RMSD (aRMSD) [45] of the 10 best poses returned for each docking function and the number of best docked poses with a RMSD value equal or below to 2 Å were calculated.

3. Results

3.1. Pose prediction

The two different CXCR4 co-crystallized ligands, IT1t and CVX15, were selfdocked into their respective protein structures using GoldScore, ChemScore, GoldScore rescored with ChemScore, Glide, Surflex and Ligandfit docking functions. Table 3 shows the best RMSD poses returned for each docking function and each PDB, the calculated average RMSD (aRMSD) of the 10 best poses, and the number of docked poses with a RMSD value equal or below to 2 Å.

The main weakness of using RMSD to evaluate the pose prediction is its dependency to the molecular size [46]. This is well noted for the cyclic peptide ligand, CVX15, in PDB 3OE0. The RMSD values obtained for 3OE0 are clearly higher than the results obtained for the small organic ligand IT1t co-crystallized in the rest of PDBs.

Comparing the results for PDBs whose cognate ligand is IT1t, it can be observed that PDB 3ODU returns the lowest aRMSD value (4.0 Å), as well as the highest number of best docked poses with a RMSD equal or below to 2 Å. In addition, PDB 3ODU is the receptor structure with the highest crystallographic resolution (2.5 Å).

3.2. Docking-based virtual screening performance

Pérez-Nueno et al. test set of actives and decoys was docked against all five CXCR4 PDBs and the CXCR4 homology model using the aforementioned docking functions. Docked poses were ranked attending to their docking score. Fig. 7 shows the ROC plots for each PDB and each scoring function. AUC values are shown in Table 5a. Tables 4a and 4b show the early recovery performance in terms of EF at 1%, 5% and 10% of the screened database and the percentage of true positives selected at 1%, 5% and 10% of false positives, respectively.

It can be observed that the ROC curves for the CXCR4 homology model obtained using Ligandfit scoring functions do not arrive until 100% of screened database. Discovery Studio is very sensitive to the size of the ligand, the geometry of the binding pocket, and the definition of the binding pocket sphere to retrieve accurate protein–ligand interaction energies. Hence, if good interactions cannot be found with a given definition of the binding pocket for a determined ligand, the software will not return a docking score for that ligand. When defining the CXCR4 binding pocket as for the rest of the docking software (see Section 2), Discovery Studio did not retrieve results for 200 out of the 248 actives. Hence, in order to improve hits retrieval, the binding site of the CXCR4 homology model was defined first into two and after into three partition levels using Discovery Studio (Fig. 8). Discovery Studio partition levels divide randomly one binding site into a specified number of subsites. In this manner, the docking engine Ligandfit explores each subsite and all the different combinations of them. Consequently when *n* subsites are defined, the test set is docked *n* factorial times along the binding site. Docking-based VS was carried out exploring in a single run every sub-site, and also the combinations of

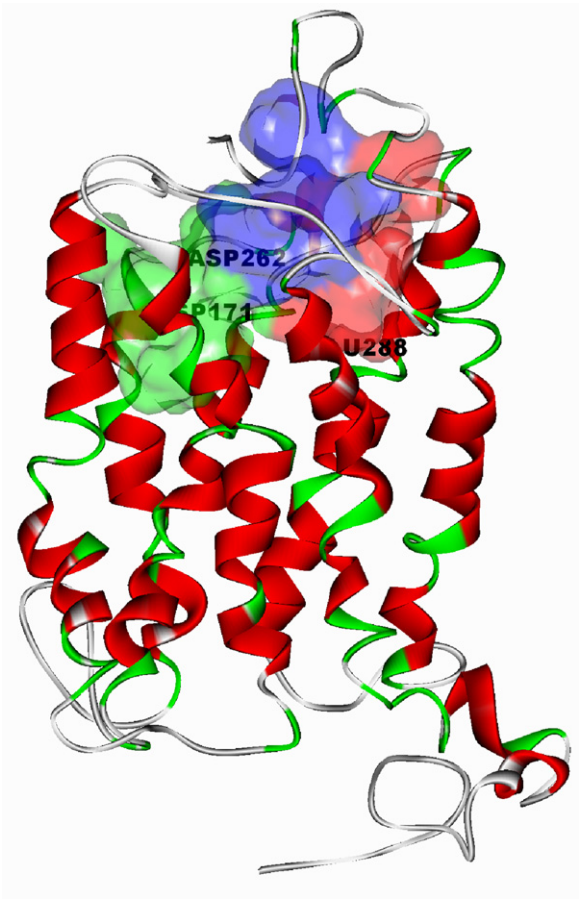

Fig. 8. Definition of three sub-sites (green, blue, and red) in the CXCR4 homology model using Discovery Studio. LigandFit assays to dock every pose into the three subsites (green, blue, and red) and also into the combination of 2 sub-sites (green–blue, green–red and blue–red). (For interpretation of the references to color in this figure legend, the reader is referred to the web version of the article.)

two different sub-sites when three sub-sites were defined. Hits retrieval and VS performance improved significantly when defining three sub-sites with respect to defining only one or two sub-sites. The Ligandfit ROC curves shown in Fig. 7 for the CXCR4 homology model represent the results when dividing the pocket in three subsites. The fact that dividing the CXCR4 pocket in sub-sites increases the VS performance agrees with recent published literature which support the fact that at least two binding sub-sites exist [12–14] in the main CXCR4 binding pocket located between ECL2 and the N-terminus, and also with the fact that antagonists like the bicyclam AMD3100, the monocyclam AMD3465, and the non-cyclam AMD11070 bind to CXCR4 in three different binding modes [47]. The distribution of actives, when those were docked into the three sub-sites, was mainly between the pockets defined by sub-sites 1-2 and 2-3. 100 actives were docked in sub-site 1-2 and 116 actives were docked in sub-site 1-3. In pockets defined by sub-sites 1-3, 1-1, and 2-2, only 9, 2, and 1 actives were docked, respectively. In addition, if we classify the compounds retrieved in each pocket subsite by chemotype families, we retrieve 52% of AMD derivates, 37% of tetrahydro-quinolinamides, 21% of macrocycles and 35% of KRH derivates in the pocket defined by sub-sites 1-2, and 32% of AMD derivates, 58% of tetrahydro-quinolinamides, 58% of macrocycles and 35% of KRH derivates in the pocket defined by sub-sites 2-3.

In general, ROC plot analysis shows that the docking-based VS is selective in choosing ligands from decoys for the retrospective test set. Concretely, comparing early recovery values obtained for all PDBs, it can be observed that PDB 3OE6 obtains the highest top

Table 3
Pose prediction analysis when cognate ligands were selfdocked into their respective protein structures. Data in bold represents the best values obtained for each docking function when comparing all five structures. PDB 3OE0 shows the highest RMSD values due to its higher molecular weight.

Pose prediction	PDB	3ODU	3OE0	3OE6	3OE8	3OE9
GoldScore	Best RMSD pose	**1.0**	9.2	5.4	6.5	5.7
	aRMSD	**3.9**	14.0	6.5	7.9	7.3
	No. poses ≤2 Å	**3**	0	0	0	0
ChemScore	Best RMSD pose	**2.2**	14.7	4.1	4.6	5.1
	aRMSD	**2.7**	15.3	6.1	5.2	6.1
	No. poses ≤2 Å	0	0	0	0	0
GoldScore and ChemScore	Best RMSD pose	**1.0**	9.8	4.2	3.6	6.2
	aRMSD	**3.7**	13.9	5.4	7.9	7.6
	No. poses ≤2 Å	**4**	0	0	0	0
Glide	Best RMSD pose	4.3	–[a]	**1.5**	**1.5**	3.1
	aRMSD	4.8	–	5.3	**3.8**	5.1
	No. poses ≤2 Å	0	–	1	**2**	0
Surflex TotalScore	Best RMSD pose	**3.2**	13.7	3.8	4.0	2.4
	aRMSD	**4.8**	22.9	5.2	5.4	4.3
	No. poses ≤2 Å	0	0	0	0	0
LigandFit	Best RMSD pose	**2.4**	5.3	2.6	3.0	5.3
	aRMSD	**4.5**	6.0	4.7	5.2	6.0
	No. poses ≤2 Å	0	0	0	0	0
AutoDock Vina	Best RMSD pose	**2.3**	–[a]	3.2	3.5	5.0
	aRMSD	**5.1**	–	7.0	5.6	6.6
	No. poses ≤2 Å	0	–	0	0	0
	Mean aRMSD	**4.5**	14.2	5.7	6.0	6.2

[a] Ligand CVX15, co-crystallized in PDB 3OE0, with more than 56 rotatable bonds exceeds Glide and AutoDock Vina docking requirements.

EF values (values shown in bold in Table 4a) and also the highest aEF (11.2 at 1% of screened database, 7.5 at 5% and 5.4 at 10% of database screened) taking into account all scoring functions used, even scoring functions with poorest results. Equally, the average percentage of true positives (Table 4b) returned at 1%, 5% and 10% of false positives is favorable for PDB 3OE6 (19.3% of true positives at 1% of false positives, 44.1% at 5% and 57.2% at 10% of false positives) among all scoring functions.

Comparing AUC and pAUC data values at 1%, 5% and 10% of screened decoys for all PDBs, it can be observed that PDB 3OE6 obtains also the highest top AUC and pAUC values (values shown in bold in Tables 5a and 5b), the highest aAUC value (0.82) and the highest average pAUC values (0.56 at 1%, 0.64 at 5% and 0.69 at 10% of decoys screened, respectively) among all scoring functions.

Enrichment factors, early recovery, AUC and pAUC results for the homology model (HomolMod) are also shown in Tables 4a, 4b, 5a and 5b, respectively.

3.3. Scaffold retrieval analysis

Pérez-Nueno et al. test set contains 248 actives from four chemotype families: AMD derivates [29,48], tetrahydro-quinolinamines [49,50], macrocycles [51,52] and KRH derivates [53,54]. To evaluate the ability of the docking protocol to retrieve these diverse scaffold families, we analyzed the percentage of actives returned by the scoring functions attending to its intrinsic chemotype classification at 1%, 5%, and 10% of screened database. Moreover, to assess how selective is the scaffold retrieval we chose PDB 3OE6 as CXCR4 working structure, being the most powerful in terms of aAUC, pAUC, and early recovery performance. Fig. 9 shows the scaffold retrieval rates. It can be observed that at 1% of screened database all four CXCR4 scaffolds are found. Only for tetrahydro-quinolinamines and for KRH derivates, one and four scoring functions respectively, did not retrieve any compound at 1% of screened database and at 5% of screened database only one scoring function failed to recover any KRH derivates. It is also well noted that at 5% of screened database the scoring function LigScore2 recovered more than 40% of all chemotype CXCR4 families and other scoring functions like Surflex-TotalScore, PLP1, and PMF recovered more than 30% of all CXCR4 scaffolds. Analysis at 10% of screened database revealed that on average all scaffolds were retrieved in more than 50% of their family compounds unless for tetrahydro-quinolinamines and KRH derivates whose average retrieval rate was 47.4% and 46.2%, respectively.

4. Discussion

Docking evaluation of five CXCR4 crystal structures and a CXCR4 homology model was carried out in terms of pose prediction and retrospective docking-based VS. We used representative force-field based scoring functions like GoldScore and DockScore, empirical scoring functions like ChemScore, Surflex-TotalScore, Glide, LigScore1, LigScore2, PLP1, PLP2 and Jain, and also knowledge-based scoring functions such as PMF or the hybrid knowledge-based and empirical scoring function Autodock Vina.

With respect to pose prediction, RMSD results for the top 10 binding poses retrieved for all PDBs using all aforementioned docking functions are not totally satisfactory. Average RMSD values from Table 3 are all higher than 2 Å. Only four aRMSD results reached values between 2 and 4 Å, *i.e.* with the PDB 3ODU for the scoring functions GoldScore (3.9 Å), ChemScore (2.7 Å) and GoldScore rescored with ChemScore (3.7 Å) and with the PDB 3OE8 using Glide (3.8 Å). Moreover, Table 3 also shows only four binding modes with RMSD values below 2 Å, *i.e.* for PDB 3ODU the best RMSD pose was 1.0 Å using GoldScore and GoldScore rescored with ChemScore and for PDB 3OE6 and 3OE8 we obtained in both cases 1.5 Å using Glide.

Comparing pose prediction between the PDBs it can be observed that PDB 3ODU obtains on average the most accurate results (mean aRMSD of 4.5 Å) using as scoring functions GoldScore, ChemScore and GoldScore rescored with ChemScore. As we stated before, it is necessary to take into account that RMSD metric depends on the molecular size of the ligand to dock, and therefore results obtained from docking the peptidic ligand CVX15 (molecular weight of

Table 4a
Early recovery performance expressed by the enrichment factor at 1%, 5%, and 10% of the screened database. The best enrichment factor values obtained for each scoring function are shown in bold. PDB 3OE6 retrieves the best enrichment factors across all docking approaches. Moreover, the highest enrichment factor value at 1% of the database screened was also obtained for structure 3OE6 (19.7).

Enrichment factors	% screened database	3ODU	3OE0	3OE6	3OE8	3OE9	HomolMod
GoldScore	1	1.2	4.5	3.3	2.9	1.6	**15.3**
	5	1.8	3.3	2.5	2.6	1.5	**9.0**
	10	1.9	3.0	1.9	2.3	1.6	**5.7**
ChemScore	1	3.6	3.2	10.5	**15.3**	6.9	7.0
	5	2.6	4.1	7.0	**8.4**	4.1	5.7
	10	2.3	3.1	5.1	**5.2**	3.4	4.7
GoldScore and ChemScore	1	3.2	2.8	5.6	6.0	9.3	**14.5**
	5	3.0	4.3	4.8	4.5	5.3	**7.8**
	10	2.7	3.6	3.8	3.2	4.0	**4.7**
Glide	1	2.8	**18.9**	8.5	8.5	15.7	4.0
	5	4.3	**12.4**	5.4	5.4	10.3	2.4
	10	4.6	**7.6**	4.2	4.2	6.5	1.7
Surflex TotalScore	1	9.7	9.2	**15.1**	8.4	10.1	9.6
	5	5.4	7.2	**9.2**	7.9	8.7	6.3
	10	3.5	5.9	**6.8**	6.5	6.6	4.9
LigandFit DockScore	1	18.7	19.3	**19.7**	19.2	15.8	9.5
	5	11.7	**15.5**	12.4	12.5	8.3	4.5
	10	8.3	**9.4**	8.3	8.2	6.2	3.6
LigandFit LigScore1	1	14.7	2.0	**19.7**	9.4	12.9	18.1
	5	8.6	4.9	**12.4**	6.6	4.7	9.5
	10	6.1	4.0	**8.3**	4.5	4.9	6.0
LigandFit LigScore2	1	15.5	6.4	14.8	11.4	12.9	**18.5**
	5	**11.5**	7.0	11.3	8.7	4.7	9.3
	10	**8.0**	6.6	**8.0**	6.9	5.5	6.2
LigandFit PLP1	1	9.8	8.1	**10.3**	9.0	8.3	4.1
	5	8.2	6.7	**8.5**	7.9	6.8	2.8
	10	6.4	5.9	**6.7**	6.2	5.9	1.7
LigandFit PLP2	1	**9.8**	5.6	9.4	7.3	7.9	2.9
	5	6.7	5.7	7.4	**7.6**	5.5	1.6
	10	5.4	5.4	**5.8**	**5.8**	4.4	1.0
LigandFit Jain	1	10.2	6.4	12.3	3.7	12.9	**19.3**
	5	5.7	3.0	5.4	2.6	6.4	**9.7**
	10	4.0	2.3	3.4	1.9	4.4	**6.6**
LigandFit PMF	1	5.7	3.6	**10.7**	7.3	6.2	0.4
	5	3.9	3.2	**7.3**	5.0	4.3	0.5
	10	3.0	3.0	**5.4**	4.2	3.6	0.8
AutoDock Vina	1	2.4	0.8	**5.1**	2.0	2.8	0.4
	5	1.9	1.2	**3.6**	1.8	2.1	1.6
	10	1.8	1.1	**3.0**	1.4	1.6	1.6
Average EF for each PDB	1	8.3	6.5	**11.2**	8.5	9.5	9.5
	5	5.8	5.6	**7.5**	6.3	5.6	5.4
	10	4.5	4.3	**5.4**	4.7	4.5	3.8

2138.6 g/mol), co-crystallized in PDB 3OE0, cannot be directly compared with the results obtained for the small ligand IT1t (molecular weight of 406.7 g/mol), co-crystallized in the rest of PDBs.

With regard to the retrospective docking-based VS, we used Pérez-Nueno et al. test set of 248 different actives from four different CXCR4 antagonist families to guarantee chemotype diversity, and 4696 decoys from the Maybridge Screening Collection with similar properties to the actives. It is worth noting the relevance in choosing actives from different chemotype families in order to evaluate well the potency of the scoring functions according to the diversity of ligands [55].

As aforementioned, only PDBs 3ODU and 3OE0 contain cocrystallized water molecules. The convenience of maintaining water molecules into the protein structure was analyzed (see Supplementary Fig. 2 and Tables 1, 2. PDB 3ODU with and without waters molecules was compared with PDB 3OE6 (the most selective VS model). Supplementary Fig. 2 shows that ROC plots for LigandFit scoring functions do retrieve neither the 100% of all actives nor 100% of decoys for PDB 3ODU with water molecules. This observation agreed with the VS results obtained for PDB 3OE0 containing water molecules, where no molecule was retrieved for LigandFit Scoring functions.

Comparison of the early recovery data (Supplementary Tables 1 and 2) obtained for structures with and without water molecules shows that GoldScore, GoldScore rescored with ChemScore, Glide, Surflex and Autodock Vina retrieve slightly higher early recovery values for 3ODU with water molecules ($3ODU_{water}$) than when water molecules were removed (3ODU). However, for ChemScore and the seven LigandFit scoring functions, early recovery values for 3ODU outperform $3ODU_{water}$. Hence, removing water molecules from CXCR4 structures 3ODU and 3OE0 does not seem a rough approximation given that the VS early recovery values obtained when comparing $3ODU_{water}$ and 3ODU are nearly equal, or in some cases better, for 3ODU without water molecules.

Analyzing the data obtained from the retrospective docking-based screenings (Fig. 7 and Tables 4a, 4b, 5a and 5b), we can

Table 4b
Early recovery performance expressed as percentage of actives recovered when 1%, 5%, and 10% of decoys were respectively selected. Values in bold represent the best percentages obtained when comparing all structures for each scoring function.

% true positives	% false positive screened	3ODU	3OE0	3OE6	3OE8	3OE9	HomolMod
GoldScore	1	1.6	6.0	3.2	3.2	1.6	**34.7**
	5	9.3	18.1	12.5	13.3	7.7	**52.0**
	10	21.4	32.7	19.0	25.0	16.1	**61.3**
ChemScore	1	4.0	3.2	15.3	**30.6**	8.9	10.5
	5	14.5	23.8	40.7	**48.0**	23.8	35.9
	10	24.6	31.9	52.8	**54.4**	35.5	52.0
GoldScore and ChemScore	1	4.4	2.8	8.1	6.9	12.1	**24.2**
	5	16.9	24.6	27.0	24.2	29.4	**43.1**
	10	28.6	39.1	43.1	33.5	40.3	**51.2**
Glide	1	3.2	**54.4**	12.1	12.1	34.7	6.0
	5	29.8	**75.0**	33.9	33.9	60.1	12.9
	10	56.0	**83.1**	46.4	46.4	71.4	17.3
Surflex TotalScore	1	13.6	13.6	**32.5**	11.5	18.1	13.2
	5	29.2	49.8	**60.9**	48.6	56.0	39.1
	10	39.5	65.8	73.7	**77.0**	**77.0**	53.9
LigandFit DockScore	1	44.1	**77.4**	49.6	49.0	26.4	12.1
	5	78.5	**93.1**	77.4	78.1	54.9	24.6
	10	90.7	**96.0**	93.5	89.5	79.3	41.9
LigandFit LigScore1	1	26.3	2.0	20.2	17.0	19.1	**38.7**
	5	**55.1**	30.6	45.2	36.0	24.4	51.6
	10	**66.8**	45.6	56.0	50.6	55.7	64.5
LigandFit LigScore2	1	**42.1**	6.9	34.3	24.7	19.1	35.5
	5	**77.3**	52.4	76.6	61.5	24.4	57.3
	10	**94.3**	80.2	90.3	81.8	78.9	69.4
LigandFit PLP1	1	**18.6**	12.1	18.1	10.9	12.6	4.4
	5	56.7	48.8	**57.3**	49.4	44.7	13.7
	10	71.3	70.2	**75.8**	72.5	67.1	19.0
LigandFit PLP2	1	14.2	6.5	**17.7**	13.8	10.6	3.6
	5	41.7	39.1	47.6	**47.8**	32.1	8.1
	10	60.7	64.5	65.3	**66.4**	47.2	9.7
LigandFit Jain	1	14.6	7.3	17.3	4.0	20.3	**37.1**
	5	30.4	15.7	30.6	13.4	38.2	**58.1**
	10	41.7	24.6	36.7	19.0	46.7	**73.0**
LigandFit PMF	1	6.9	6.9	**17.7**	10.5	8.1	0.4
	5	21.5	21.5	**44.8**	28.3	26.8	2.4
	10	32.4	32.4	**60.5**	47.0	39.8	7.7
AutoDock Vina	1	2.4	0.81	**5.2**	2.0	2.8	0.4
	5	9.7	6.05	**19.4**	10.5	10.5	8.9
	10	18.2	11.29	**30.7**	14.1	18.2	16.1
Average % true positives for each PDB	1	15.1	15.4	**19.3**	15.1	15.0	17.0
	5	36.2	38.4	**44.1**	37.9	33.3	31.4
	10	49.7	52.1	**57.2**	52.1	51.8	41.3

Table 5a
AUC values calculated from the ROC plot for all the CXCR4 PDBs and the CXCR4 homology model. Values in bold represent the best AUC values obtained when comparing all structures for each scoring function.

AUC	3ODU	3OE0	3OE6	3OE8	3OE9	HomolMod
GoldScore	0.62	0.70	0.77	0.80	0.60	**0.83**
ChemScore	0.72	0.70	0.61	0.63	0.71	**0.81**
GoldScore and ChemScore	0.72	0.69	**0.79**	0.71	0.74	0.75
Glide	0.80	**0.95**	0.82	0.91	0.89	0.26
Surflex TotalScore	0.75	0.88	0.91	0.91	**0.92**	0.74
LigandFit DockScore	0.95	**0.99**	0.96	0.95	0.91	0.52
LigandFit LigScore1	0.88	0.80	0.84	0.83	**0.85**	0.75
LigandFit LigScore2	**0.96**	0.93	**0.96**	0.93	0.92	0.77
LigandFit PLP1	0.90	0.89	**0.91**	0.90	0.86	0.43
LigandFit PLP2	0.85	0.88	0.88	0.88	**0.92**	0.31
LigandFit Jain	0.71	0.59	0.62	0.47	0.74	**0.79**
LigandFit PMF	0.73	0.76	**0.85**	0.79	0.78	0.46
AutoDock Vina	0.60	0.47	**0.71**	0.60	0.64	0.66
aAUC for each PDB	0.78	0.79	**0.82**	0.79	0.81	0.62

Table 5b
Partial area indexes calculated from the pAUC values at 1%, 5% and 10% of decoys retrieved for all the CXCR4 PDBs and the CXCR4 homology model. Values in bold represent the best partial area indexes obtained when comparing all structures for every scoring function.

pAUC	% false positive Screened	3ODU	3OE0	3OE6	3OE8	3OE9	Homolog. Model
GoldScore	1	0.51	0.51	0.55	**0.61**	0.52	**0.61**
	5	0.53	0.55	0.63	0.68	0.56	**0.70**
	10	0.55	0.58	0.67	0.70	0.59	**0.73**
ChemScore	1	0.50	0.51	0.50	0.51	0.51	**0.53**
	5	0.51	0.54	0.52	0.52	0.51	**0.59**
	10	0.53	0.57	0.53	0.54	0.53	**0.64**
GoldScore and ChemScore	1	0.51	0.51	0.52	0.52	0.54	**0.59**
	5	0.54	0.55	0.57	0.56	0.59	**0.66**
	10	0.56	0.59	0.61	0.59	0.62	**0.68**
Glide	1	0.50	**0.71**	0.54	0.59	0.62	0.51
	5	0.55	**0.80**	0.60	0.70	0.72	0.53
	10	0.62	**0.85**	0.63	0.76	0.77	0.54
Surflex TotalScore	1	0.54	0.54	**0.60**	0.53	0.55	0.54
	5	0.59	0.63	**0.71**	0.64	0.67	0.61
	10	0.62	0.70	**0.77**	0.72	0.75	0.66
LigandFit DockScore	1	0.66	**0.77**	0.70	0.70	0.60	0.54
	5	0.79	**0.91**	0.80	0.81	0.68	0.58
	10	0.86	**0.94**	0.86	0.86	0.74	0.61
LigandFit LigScore1	1	0.59	0.50	0.56	0.54	0.56	**0.65**
	5	0.68	0.56	0.64	0.61	0.60	**0.71**
	10	**0.74**	0.61	0.69	0.65	0.64	**0.74**
LigandFit LigScore2	1	0.62	0.52	**0.60**	0.56	0.57	0.64
	5	0.78	0.61	**0.75**	0.68	0.60	0.71
	10	0.85	0.72	**0.83**	0.77	0.67	0.76
LigandFit PLP1	1	**0.55**	0.53	**0.55**	0.54	0.54	0.51
	5	**0.66**	0.61	**0.66**	0.64	0.62	0.53
	10	0.73	0.70	**0.74**	0.72	0.70	0.53
LigandFit PLP2	1	0.54	0.52	**0.55**	0.53	0.53	0.51
	5	0.62	0.58	**0.64**	**0.64**	0.59	0.51
	10	0.68	0.66	0.70	**0.71**	0.63	0.51
LigandFit Jain	1	0.55	0.52	0.56	0.51	0.57	**0.67**
	5	0.60	0.54	0.60	0.53	0.63	**0.73**
	10	0.63	0.56	0.62	0.54	0.66	**0.77**
LigandFit PMF	1	0.52	0.51	**0.55**	0.53	0.52	0.50
	5	0.55	0.53	**0.63**	0.58	0.56	0.49
	10	0.58	0.56	**0.69**	0.62	0.60	0.49
AutoDock Vina	1	0.50	0.50	**0.51**	0.50	0.51	0.50
	5	0.49	0.50	**0.54**	0.49	0.52	0.50
	10	0.52	0.50	**0.57**	0.52	0.53	0.51
Average pAUC for each PDB	1	0.55	0.55	**0.56**	0.55	0.55	**0.56**
	5	0.61	0.61	**0.64**	0.62	0.60	0.60
	10	0.65	0.66	**0.69**	0.67	0.65	0.63

affirm that retrospective docking results obtained for all CXCR4 PDBs are completely satisfactory in terms of early recovery. All PDBs obtained several EF values equal or higher than 10 at 1% of screened database (Table 4a). Principally, for PDB 3OE6, eight scoring functions reached EF values up to 10 and the average EF of all scoring functions used to dock this PDB was 11.2. Discarding the three scoring functions which retrieve the poorest scores (GoldScore, GoldScore rescored with ChemScore and AutoDock Vina) the aEF rises to 13.1.

Regarding the scoring functions that retrieve the best early recovery performance, scoring function DockScore from LigandFit performed the best, showing EF values close to 20 for all PDBs at 1% of screened database (Table 4a), unless for PDB 3OE9 (15.8). The DockScore scoring function is a force field based approximation that estimates the energy of interaction by summing the internal energy of the ligand and the ligand–receptor interaction energy. In addition, the ligand–receptor interaction energy is taken as the sum of the van der Waals energy and electrostatic energy.

Moreover, the majority of scoring functions from LigandFit, as well as Surflex and Glide retrieved also very good early recovery results. Hence, Ligandfit from Discovery Studio, Surflex from Sybyl and Glide from Schroedinger docking packages are well suited to deal with CXCR4 docking-based VS.

Evaluation of the ROC plots (Fig. 7), and the corresponding AUC data (Table 5a) and pAUC (Table 5b) also show good performance of the different scoring functions for the PDBs complexed with both the peptide antagonist and the IT1t small ligand. LigandFit functions, Glide and Surflex scoring functions returned the most selective ROC plots and the highest AUC values in all retrospective dockings. It should be noted that peptidic ligands often generate induced fit conformational changes into the protein structure, leading, consequently, to structural changes into the binding site. However, docking the test set against PDB 3OE0 and using the scoring function LigandFit, we obtained the best AUC result (0.99) and the best pAUC values at 1% (0.77), at 5% (0.91), and at 10% (0.94) of decoys retrieved. Consistently to these pAUC values, the early

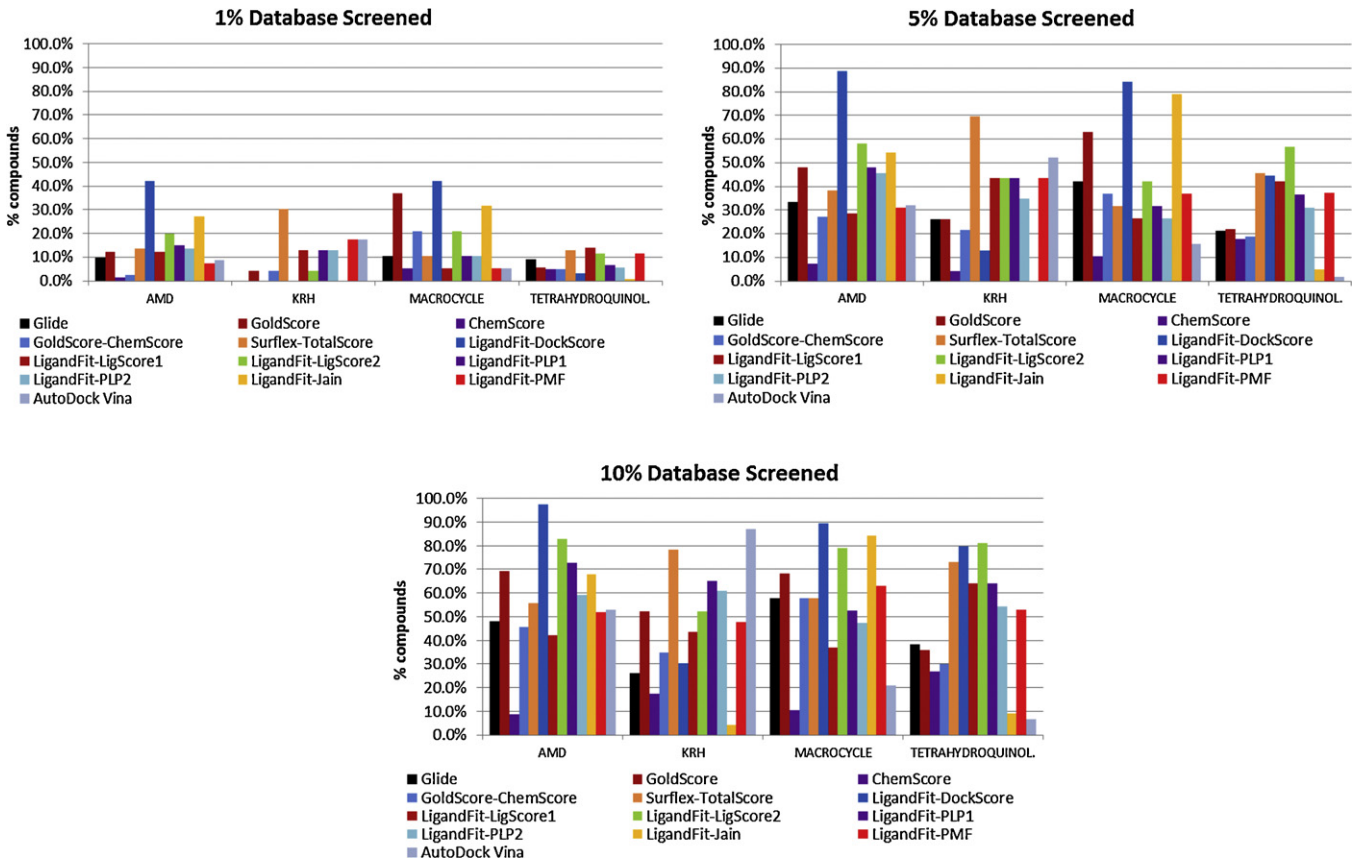

Fig. 9. Scaffold diversity retrieval plots for PDB 3OE6. These graphics show the percentage of actives by chemotype family retrieved using all different scoring functions (bars in colors) at 1%, 5% and 10% of the screened database, respectively. (For interpretation of the references to color in this figure legend, the reader is referred to the web version of the article.)

recovery was also the highest (77.4% of actives at 1% of recovered decoys) along all retrospective dockings.

If we compare the ROC plots and their corresponding AUC values by PDB (Table 5a), all PDBs obtained average AUC values (aAUC) around 0.8, corresponding the highest aAUC value to PDB 3OE6 (0.82). Also, the PDB 3OE6 obtained the best AUC values (Table 5a in bold) when compared with the AUC values achieved for the rest of PDBs. Comparison of the early recovery and AUC values obtained for each scoring function and all the structures shows that PDB 3OE6 again returns the most selective results for GoldScore rescored with ChemScore, LigandFit LigScore2, LigandFit PLP1, LigandFit PMF and AutoDock Vina scoring functions. Attending to these results, we chose PDB 3OE6 for a scaffold retrieval analysis using the scoring functions selected in this work. This analysis shows that all four chemotype families were retrieved for all scoring functions at 10% of the screened database and only one scoring function did not retrieve KRH compounds at 5% of screened database. Therefore, scaffold retrieval results obtained for PDB 3OE6 are also completely satisfactory.

Comparing the docking-based VS results obtained for the CXCR4 homology model with the ones obtained for all the CXCR4 PDBs, it can be observed that the homology model captures as well as the PDB complexes the early recovery performance. Good enrichment factors at 1% of the screened database and good percentage of true positives at 1% of decoys were retrieved for the scoring functions: GoldScore (15.3 and 34.7%) and GoldScore rescored with ChemScore (14.5 and 24.2%), LigandFit LigScore1 (18.1 and 38.7%), LigandFit LigScore2 (18.5 and 35.5%) and LigandFit Jain (19.3 and 37.1%). On average, early recovery results were similar and in some cases even better than those obtained for the crystallized structures. Nevertheless, generally poor early recovery results were achieved using the scoring functions: Glide, LigandFit PLP1, LigandFit PLP2, LigandFit PMF and AutoDock Vina. Additionally, for the homology model, it was observed that early recovery values became less selective when increasing the percentage of screened database.

In the same way when comparing the ROC plots for the homology model and the crystal structures it can be observed that the highest average pAUC value at 1% of retrieved decoys (Table 5b) was achieved by the homology model as well as by the 3OE6 PDB (average pAUC of 0.56). Moreover, average pAUC values at 5% and 10% of retrieved decoys for the homology model were very similar to the values obtained for the crystal structures.

Hence, the homology model performed as well as the crystal structures in the first percentages of database screened, which suggests that using an homology model created from a template crystallized with a representative ligand may be a decent approach to separate members of a particular inhibitor class from inactives in virtual screening experiments. This observation is consistent with several papers that support the use of homology models for GPCR [56,57] predictions and protein kinases VS [58]. Vilar et al. support the notion that homology models often provide a reasonable framework for discussing experimental data. They state that crystal structures are only static representations of proteins and neglecting protein flexibility by using only one rigid representation of the target has been shown to adversely affect virtual screening performance. They claim that receptor ensemble docking, a method where docking is performed on several distinct structures and the results are subsequently combined, has been successfully used to account for protein flexibility in virtual screening campaigns [56].

Hence, combining docking results obtained using different CXCR4 crystal structures or even different CXCR4 homology models could help to account for protein flexibility and to improve VS results. Furthermore, it is also worth mentioning that if a particular protein family has a greater degree of induced fit upon ligand binding, then homology models created from a template with an appropriate ligand bound will produce better docking results than a crystal structure with no ligand or a dissimilar ligand bound [56].

In summary, although the homology model performs as well as the crystal structures in the first percentages of database screened the total VS performance shows a limited predictive power. CXCR4 is generally a target difficult to dock. Retrospective docking results and binding mode prediction are not completely satisfactory. Binding mode analyses of the docked poses onto the CXCR4 homology model allowed us to hypothesize multiple binding sub-sites in CXCR4 binding pocket. This hypothesis could explain the difficulty in retrieving good receptor-based VS results. Recent studies show that there are several notable differences in the binding mode of the monocyclam (such as AMD3465), bicyclam (such as AMD3100) and non-cyclam (such as MX122) antagonists [10,12–14]. Moreover, recent literature suggests that the CXCR4 conformation stabilized *i.e.* by AMD3100 differs slightly from the one stabilized by AMD3465, mainly in the orientation of TM7. This may explain the improved efficacy of AMD3465 over AMD3100 in inhibiting the action of CXCL12 [13].

Furthermore, CXCR4 flexibility makes also difficult to get good docking results. For example, by including receptor backbone flexibility, it is possible to consolidate all the mutation data pertaining to the binding of the cyclam compounds [14]. Techniques that deal with "difficult targets", that is to say targets with multiple binding sites or multiple binding modes, have recently appeared in order to improve the screening performance, such as consensus shape screening [59–61].

As expected, according to the experiment carried out (selfdocking of the two different CXCR4 co-crystallized ligands, IT1t and CVX15, into their respective protein structures using different scoring functions), the highest resolution structures performed the best in the compound pose prediction analysis. However, regarding the docking-based VS performance, it turned out that the lowest resolution structure, 3OE6, provided the best early enrichment of the actives in the screening dataset. This result leads to the debate of prioritizing conformational selection or induced fit concepts. The majority of active ligands compiled from the literature are just known to bind CXCR4, without an exact idea of their binding mode. Taking this into account, together with the fact that CXCR4 protein is known to be an allosteric transmembrane protein [62,63], leads to the hypothesis that the majority of active ligands in our compiled database bind in a more stable mode within the lowest resolution conformation in the light of our early recovery docking enrichment results. CXCR4 structures can be crystallized in slightly different conformations, regardless of the crystal resolution, which captures in some way the induced fit binding capacity of the protein. We can have two CXCR4 crystal complexes at the same resolution with different interactions in the binding pocket [64] (*i.e.* 3OE8 and 3OE9 structures, see Fig. 3) or two different resolution CXCR4 dimers with different interactions (*i.e.* 3ODU and 3OE9, see Fig. 3) which can give us an idea of the allosteric interactions. Therefore, given the light of the results in this study, we hypothesize that the lowest resolution CXCR4 crystal structure describes better the CXCR4 induced fit binding effect, allowing the wide range of different active ligand scaffold families to be better accommodated in different pocket subsites in 3OE6. Our homology model also shares this behavior of 3OE6, which is able to accommodate the wide range of actives in different pocket subsites retrieving good early recovery values. Hence, it is necessary to take a compromise when performing docking based virtual screening on allosteric proteins between choosing a higher resolution crystal structure or a lower resolution crystal structure but with a conformation describing better the induced fit mechanism of the protein. Moreover, if the induced fit effect is significantly important, it might be even better to use a good model (or good homology model if crystal structures are not available) built to account for protein flexibility, *i.e.* by consensus shape screening and receptor ensemble docking, using templates with an appropriate ligand bound. Supplementary Fig. 3 shows a comparison between the binding pockets of the highest (3ODU) and lowest (3OE6) resolution CXCR4 crystal structures used in this study in terms of H bonding, lipophilic potential, and electrostatic potential surface maps. Moreover, a detailed binding pocket interaction map showing the different interactions listed in Fig. 3 is shown for both 3ODU and 3OE6 structures. The H bonding surface map is similar for both structures, however the lowest resolution structure seems to have a bigger and more defined hydrophobic binding pocket central region surrounded by high electronegativity areas (see hydrogen bonding surface map on the left), which corresponds to the brown high lipophilic region in the lipophilic potential surface map, and a bigger and central blue region in the electrostatic potential map. The different binding pocket interactions between both structures are mainly between the residues Glu32, Lys38, Ala98, His113 and Arg188.

5. Conclusions

In the present study we have compared and evaluated for the first time all CXCR4 structures published by Wu et al. together with our previously published CXCR4 rhodopsin-based homology model under the point of view of their receptor based virtual screening performance.

With the aim of doing an evaluation that guarantees diversity during the global process we used Pérez-Nueno et al. test set of 248 known actives comprising four different chemotypes [43] of inhibitors. Additionally, we have used different kinds of scoring functions, attending to the nature of the computation algorithm, to dock our previously reported CXCR4 homology model and different CXCR4 structures co-crystallized either with a small organic molecule or a peptide antagonist.

With regard to pose prediction, results are not completely satisfactory. Binding modes obtained from the different dockings seem not to be accurate enough.

Nevertheless, retrospective docking analysis shows a good selection of known CXCR4 binders from decoys when defining a binding pocket delimited by residues Asp171, Asp262, and Glu288. In a similar manner, the homology model shows high selectivity in the classification of actives against decoys mainly in the first percentages of database screened. A detailed analysis of the retrospective docking results using the CXCR4 homology model in Discovery Studio allows us to hypothesize the existence of at least two binding sub-sites in CXCR4 binding pocket.

Summarizing the docking-based VS performance, we found that the crystal structure (3OE6) retrieved the most accurate results, especially regarding the early recovery (aEF of 11.2 at 1% of decoys screened) and the ROC plot analysis (aAUC of 0.82), despite being the lowest resolution structure (3.2 Å). Moreover, scaffold retrieval analysis of PDB 3OE6 confirmed that all chemotype families used in this study were early recovered for all scoring functions. It is also worth noting that enrichment factors and AUC data obtained for PDB 3OE0 (co-crystallized with the peptide antagonist CVX15) are very similar to the rest of PDBs (co-crystallized with the small ligand IT1t). Hence, the fact that peptidic ligands often generate induced fit conformational changes into the protein structure seems not to affect in this case the majority of VS results.

Overall, herein we analyze in depth the receptor-based VS performance of the five recent crystallized CXCR4 structures, along with our previously published CXCR4 rhodopsin-based homology model. We propose PDB 3OE6 as the most suitable crystal structure to carry on new prospective docking analyses with the maximum guarantees. We also show that our previous CXCR4 rhodopsin-based homology model discriminates actives from decoys at the first percentage of database screened as well as the crystal structures do. We hypothesize that these both structures perform well due to their capacity to capture in some way a more general induced fit conformation to which a wide range of ligands can bind due to the known CXCR4 allosteric behavior. These results support the notion that if no information is available, as it was the case of CXCR4 target years ago, homology models can be useful. Moreover, a detailed analysis of the retrospective docking results using the CXCR4 homology model in Discovery Studio allows us to hypothesize the existence of multiple binding sub-sites in CXCR4 binding pocket.

Acknowledgements

The authors thank the Servei de Disseny de Farmacs (SDF) in the Centre de Supercomputacio de Catalunya (CESCA) for providing access to the computational software used through. This work is supported by the Programa Nacional de Biomedicina (Ministerio de Educación y Ciencia, SAF2010-21617-C02-02). V.I.P.N. is grateful for a Marie Curie IEF Fellowship grant reference DOVSA 254128.

Appendix A. Supplementary data

Supplementary data associated with this article can be found, in the online version, at http://dx.doi.org/10.1016/j.jmgm.2012.06.010.

References

[1] J.C. Tilton, R.W. Doms, Entry inhibitors in the treatment of HIV-1 infection, Antiviral Research 85 (2010) 91–100.
[2] S.A. Trushin, G.D. Bren, A.D. Badley, CXCR4 tropic HIV-1 gp120 inhibition of SDF-1α-induced chemotaxis requires Lck and is associated with Cofilin phosphorylation, Open Virology Journal 4 (2010) 157.
[3] P.R. Harrigan, L. Swenson, R.A. McGovern, G.J. Pollock, The determinants and consequences of HIV coreceptor switching, HIV Medical Update 4 (2009).
[4] T. Haga, S. Takeda, G Protein-coupled Receptors: Structure, Function, and Ligand Screening, CRC Press, Boca Raton, 2005.
[5] W.T. Choi, J. An, Biology and clinical relevance of chemokines and chemokine receptors CXCR4 and CCR5 in human diseases, Experimental Biology and Medicine 236 (2011) 637–647.
[6] M. Peeters, G. van Westen, Q. Li, A. IJzerman, Importance of the extracellular loops in G protein-coupled receptors for ligand recognition and receptor activation, Trends in Pharmacological Sciences 32 (2011) 35–42.
[7] B. Wu, E.Y.T. Chien, C.D. Mol, G. Fenalti, W. Liu, V. Katritch, R. Abagyan, A. Brooun, P. Wells, F.C. Bi, Structures of the CXCR4 chemokine GPCR with small-molecule and cyclic peptide antagonists, Science 330 (2010) 1066–1071.
[8] C.A. Mosley, L.J. Wilson, J.M. Wiseman, J.W. Skudlarek, D.C. Liotta, Recent patents regarding the discovery of small molecule CXCR4 antagonists, Expert Opinion on Therapeutic Patients 19 (2009) 23–38.
[9] G. Moncunill, M. Armand-Ugon, I. Clotet-Codina, E. Pauls, E. Ballana, A. Llano, B. Romagnoli, J.W. Vrijbloed, F.O. Gombert, B. Clotet, Anti-HIV activity and resistance profile of the CXC chemokine receptor 4 antagonist POL3026, Molecular Pharmacology 73 (2008) 1264.
[10] S. Pettersson, V.I. Pérez Nueno, M.P. Mena, B. Clotet, J.A. Esté, J.I. Borrell, J. Teixidó, Novel monocyclam derivatives as HIV entry inhibitors: design, synthesis anti HIV evaluation, and their interaction with the CXCR4 co receptor, ChemMedChem 5 (2010) 1272–1281.
[11] V.I. Perez-Nueno, D.W. Ritchie, J.I. Borrell, J. Teixido, ChemInform abstract: clustering and classifying diverse HIV entry inhibitors using a novel consensus shape-based virtual screening approach: further evidence for multiple binding sites within the CCR5 extracellular pocket, Journal of Chemical Information and Modeling 48 (2008) 2146–2165.
[12] S.P. Kawatkar, M. Yan, H. Gevariya, M.Y. Lim, S. Eisold, X. Zhu, Z. Huang, J. An, Computational analysis of the structural mechanism of inhibition of chemokine receptor CXCR4 by small molecule antagonists, Experimental Biology and Medicine 236 (2011) 844–850.
[13] M.A.C. Neves, S. Simões, M.L. Sá e Melo, Ligand-guided optimization of CXCR4 homology models for virtual screening using a multiple chemotype approach, Journal of Computer-Aided Molecular Design 24 (2010) 1023–1033.
[14] A.R. Lam, S. Bhattacharya, K. Patel, S.E. Hall, A. Mao, N. Vaidehi, Importance of receptor flexibility in binding of cyclam compounds to the chemokine receptor CXCR4, Journal of Chemical Information and Modeling 51 (2010) 137–147.
[15] R. Wang, Y. Lu, X. Fang, S. Wang, An extensive test of 14 scoring functions using the PDB bind refined set of 800 protein–ligand complexes, Journal of Chemical Information and Computer Science 44 (2004) 2114–2125.
[16] O. Trott, A.J. Olson, AutoDock Vina: improving the speed and accuracy of docking with a new scoring function, efficient optimization, and multithreading, Journal of Computational Chemistry 31 (2010) 455–461.
[17] M.L. Verdonk, J.C. Cole, M.J. Hartshorn, C.W. Murray, R.D. Taylor, Improved protein–ligand docking using GOLD, Proteins: Structure, Function, and Bioinformatics 52 (2003) 609–623.
[18] R.A. Friesner, J.L. Banks, R.B. Murphy, T.A. Halgren, J.J. Klicic, T. Daniel, M.P. Repasky, E.H. Knoll, M. Shelley, J.K. Perry, Glide: a new approach for rapid, accurate docking and scoring 1. Method and assessment of docking accuracy, Journal of Medicinal Chemistry 47 (2004) 1739–1749.
[19] T.A. Pham, A.N. Jain, Customizing scoring functions for docking, Journal of Computer-Aided Molecular Design 22 (2008) 269–286.
[20] SYBYL-X 1.1, Tripos International, 1699 South Hanley Rd., St. Louis, MO 63144, USA.
[21] A. Krammer, P.D. Kirchhoff, X. Jiang, C.M. Venkatachalam, M. Waldman, LigScore: a novel scoring function for predicting binding affinities, Journal of Molecular Graphics and Modelling 23 (2005) 395–407.
[22] D.K. Gehlhaar, G.M. Verkhivker, P.A. Rejto, C.J. Sherman, D.R. Fogel, L.J. Fogel, S.T. Freer, Molecular recognition of the inhibitor AG-1343 by HIV-1 protease: conformationally flexible docking by evolutionary programming, Chemistry and Biology 2 (1995) 317–324.
[23] Y. Bustanji, M.O. Taha, A.M. Yousef, A.G. Al-Bakri, Berberine potently inhibits protein tyrosine phosphatase 1B: investigation by docking simulation and experimental validation, Journal of Enzyme Inhibition and Medicinal Chemistry 21 (2006) 163–171.
[24] V.I. Pérez-Nueno, D.W. Ritchie, O. Rabal, R. Pascual, J.I. Borrell, J. Teixido, Comparison of ligand-based and receptor-based virtual screening of HIV entry inhibitors for the CXCR4 and CCR5 receptors using 3D ligand shape matching and ligand–receptor docking, Journal of Chemical Information and Modeling 48 (2008) 509–533.
[25] I. Kufareva, M. Rueda, V. Katritch, G. Dock, R.C. Stevens, R. Abagyan, Status of GPCR modeling and docking as reflected by community-wide GPCR Dock 2010 assessment, Structure 19 (2011) 1108–1126.
[26] X. Liang, CXCR4, inhibitors and mechanisms of action, Chemical Biology and Drug Design 72 (2008) 97–110.
[27] A.P. Graves, R. Brenk, B.K. Shoichet, Decoys for docking, Journal of Medicinal Chemistry 48 (2005) 3714–3728.
[28] MOE (Molecular Operating Environment), Chemical Computing Group Inc., Montreal, Canada, 2009.
[29] S. Hatse, K. Princen, K. Vermeire, L.O. Gerlach, M.M. Rosenkilde, T.W. Schwartz, G. Bridger, E. De Clercq, D. Schols, Mutations at the CXCR4 interaction sites for AMD3100 influence anti-CXCR4 antibody binding and HIV-1 entry, FEBS Letters 546 (2003) 300–306.
[30] L.O. Gerlach, R.T. Skerlj, G.J. Bridger, T.W. Schwartz, Molecular interactions of cyclam and bicyclam non-peptide antagonists with the CXCR4 chemokine receptor, Journal of Biological Chemistry 276 (2001) 14153–14160.
[31] M.M. Rosenkilde, L.O. Gerlach, J.S. Jakobsen, R.T. Skerlj, G.J. Bridger, T.W. Schwartz, Molecular mechanism of AMD3100 antagonism in the CXCR4 receptor, Journal of Biological Chemistry 279 (2004) 3033.
[32] M.M. Rosenkilde, L.O. Gerlach, S. Hatse, R.T. Skerlj, D. Schols, G.J. Bridger, T.W. Schwartz, Molecular mechanism of action of monocyclam versus bicyclam non-peptide antagonists in the CXCR4 chemokine receptor, Journal of Biological Chemistry 282 (2007) 27354–27365.
[33] H. Tamamura, Y. Xu, T. Hattori, X. Zhang, R. Arakaki, K. Kanbara, A. Omagari, A. Otaka, T. Ibuka, N. Yamamoto, A low-molecular-weight inhibitor against the chemokine receptor CXCR4: a strong anti-HIV peptide T140, Biochemical and Biophysical Research Communications 253 (1998) 877–882.
[34] J.O. Trent, Z. Wang, J.L. Murray, W. Shao, H. Tamamura, N. Fujii, S.C. Peiper, Lipid bilayer simulations of CXCR4 with inverse agonists and weak partial agonists, Journal of Biological Chemistry 278 (2003) 47136.
[35] J. Vabenø, G.V. Nikiforovich, G.R. Marshall, Insight into the binding mode for cyclopentapeptide antagonists of the CXCR4 receptor, Chemical Biology and Drug Design 67 (2006) 346–354.
[36] T. Fawcett, An introduction to ROC analysis, Pattern Recognition Letters 27 (2006) 861–874.
[37] Y. Jiang, C.E. Metz, R.M. Nishikawa, A receiver operating characteristic partial area index for highly sensitive diagnostic tests, Radiology 201 (1996) 745.
[38] P. Sonego, A. Kocsor, S. Pongor, ROC analysis: applications to the classification of biological sequences and 3D structures, Briefings in Bioinformatics 9 (2008) 198.
[39] N.A. Obuchowski, ROC analysis, American Journal of Roentgenology 184 (2005) 364.
[40] T.A. Lasko, J.G. Bhagwat, K.H. Zou, L. Ohno-Machado, The use of receiver operating characteristic curves in biomedical informatics, Journal of Biomedical Informatics 38 (2005) 404–415.
[41] D.K. McClish, Analyzing a portion of the ROC curve, Medical Decision Making 9 (1989) 190.

[42] A.N. Jain, Bias, reporting, and sharing: computational evaluations of docking methods, Journal of Computer-Aided Molecular Design 22 (2008) 201–212.
[43] M.D. Mackey, J.L. Melville, Better than random? The chemotype enrichment problem, Journal of Chemical Information and Modeling 49 (2009) 1154–1162.
[44] A.N. Jain, A. Nicholls, Recommendations for evaluation of computational methods, Journal of Computer-Aided Molecular Design 22 (2008) 133–139.
[45] J.B. Cross, D.C. Thompson, B.K. Rai, J.C. Baber, K.Y. Fan, Y. Hu, C. Humblet, Comparison of several molecular docking programs: pose prediction and virtual screening accuracy, Journal of Chemical Information and Modeling 49 (2009) 1455–1474.
[46] J. Kirchmair, P. Markt, S. Distinto, G. Wolber, T. Langer, Evaluation of the performance of 3D virtual screening protocols: RMSD comparisons, enrichment assessments, and decoy selection––What can we learn from earlier mistakes? Journal of Computer-Aided Molecular Design 22 (2008) 213–228.
[47] R.S.Y. Wong, V. Bodart, M. Metz, J. Labrecque, G. Bridger, S.P. Fricker, Comparison of the potential multiple binding modes of bicyclam, monocylam, and noncyclam small-molecule CXC chemokine receptor 4 inhibitors, Molecular Pharmacology 74 (2008) 1485–1495.
[48] E. De Clercq, Recent advances on the use of the CXCR4 antagonist plerixafor (AMD3100 Mozobil™) and potential of other CXCR4 antagonists as stem cell mobilizers, Pharmacology and Therapeutics 128 (2010) 509–518.
[49] J.G. Catalano, K.S. Gudmundsson, A. Svolto, S.D. Boggs, J.F. Miller, A. Spaltenstein, M. Thomson, P. Wheelan, D.J. Minick, D.P. Phelps, Synthesis of a novel tricyclic 1, 2, 3, 4, 4a, 5, 6, 10b-octahydro-1, 10-phenanthroline ring system and CXCR4 antagonists with potent activity against HIV-1, Bioorganic and Medicinal Chemistry Letters 20 (2010) 2186–2190.
[50] G. Bridger, R. Skerlj, A. Kaller, C. Harwig, D. Bogucki, T.R. Wilson, J. Crawford, E.J. Mceachern, B. Atsma, S. Nan, Chemokine Receptor Binding Heterocyclic Compounds, 2004.
[51] G.J. Bridger, R.T. Skerlj, S. Padmanabhan, S.A. Martellucci, G.W. Henson, S. Struyf, M. Witvrouw, D. Schols, E. De Clercq, Synthesis and structure–activity relationships of phenylenebis (methylene)-linked bis-azamacrocycles that inhibit HIV-1 and HIV-2 replication by antagonism of the chemokine receptor CXCR4, Journal of Medicinal Chemistry 42 (1999) 3971–3981.
[52] G.J. Bridger, R.T. Skerlj, D. Thornton, S. Padmanabhan, S.A. Martellucci, G.W. Henson, M.J. Abrams, N. Yamamoto, K.D. Vreese, Synthesis and structure–activity relationships of phenylenebis (methylene)-linked bistetraazamacrocycles that inhibit HIV replication Effects of macrocyclic ring size and substituents on the aromatic linker, Journal of Medicinal Chemistry 38 (1995) 366–378.
[53] K. Ichiyama, S. Yokoyama-Kumakura, Y. Tanaka, R. Tanaka, K. Hirose, K. Bannai, T. Edamatsu, M. Yanaka, Y. Niitani, N. Miyano-Kurosaki, A duodenally absorbable CXC chemokine receptor 4 antagonist KRH-1636, exhibits a potent and selective anti-HIV-1 activity, PNAS 100 (2003) 4185–4190.
[54] T. Yamazaki, A. Saitou, M. Ono, S. Yokoyama, K. Bannai, K. Hirose, M. Yanaka, Novel Nitrogenous Compound and Use Thereof, 2003.
[55] G.L. Warren, C.W. Andrews, A.M. Capelli, B. Clarke, J. LaLonde, M.H. Lambert, M. Lindvall, N. Nevins, S.F. Semus, S. Senger, A critical assessment of docking programs and scoring functions, Journal of Medicinal Chemistry 49 (2006) 5912–5931.
[56] S. Vilar, G. Ferino, S.S. Phatak, B. Berk, C.N. Cavasotto, S. Costanzi, Docking-based virtual screening for ligands of G protein-coupled receptors: not only crystal structures but also in silico models, Journal of Molecular Graphics and Modelling 29 (2011) 614–623.
[57] L. Roumen, M. Sanders, B. Vroling, I.J.P. de Esch, J. de Vlieg, R. Leurs, J.P.G. Klomp, S.B. Nabuurs, C. de Graaf, In silico veritas: the pitfalls and challenges of predicting GPCR–ligand interactions, Pharmaceuticals 4 (2011) 1196–1215.
[58] W.M. Rockey, A.H. Elcock, Structure selection for protein kinase docking and virtual screening: homology models or crystal structures? Current Protein and Peptide Science 7 (2006) 437–457.
[59] V.I. Perez-Nueno, D.W. Ritchie, Using consensus-shape clustering to identify promiscuous ligands and protein targets and to choose the right query for shape-based virtual screening, Journal of Chemical Information and Modeling 51 (2011) 1233–1248.
[60] V.I. Pérez-Nueno, D.W. Ritchie, Applying in silico tools to the discovery of novel CXCR4 inhibitors, Drug Development Research 72 (2011) 95–111.
[61] V.I. Pérez-Nueno, D.W. Ritchie, Identifying and characterizing promiscuous targets: implications for virtual screening, Expert Opinion on Drug Discovery 7 (2012) 1–17.
[62] L.T. May, K. Leach, P.M. Sexton, A. Christopoulos, Allosteric modulation of g protein-coupled receptors, Annual Review of Pharmacology and Toxicology 47 (2007) 1–51.
[63] J.M. Janz, Y. Ren, R.J. Looby, M.A. Kazmi, P. Sachdev, A. Grunbeck, L. Haggis, D. Chinnapen, A.Y. Lin, C. Seibert, Direct interaction between an allosteric agonist pepducin and the chemokine receptor CXCR4, Journal of the American Chemical Society 40 (2011) 15878–15881.
[64] P. Maurice, M. Kamal, R. Jockers, Asymmetry of GPCR oligomers supports their functional relevance, Trends in Pharmacological Sciences 32 (2011) 514–520.
[65] J.A. Ballesteros, H. Weinstein, Integrated methods for the construction of three-dimensional models and computational probing of structure–function relations in G protein-coupled receptors, Methods in Neurosciences 25 (1995) 366–428.